Innovative Systems Design and Engineering
ISSN 2222-1727 (Paper) ISSN 2222-2871 (Online) DOI: 10.7176/ISDE
Vol.10, No.4, 2019

Optimization Design and Development of Sensing Coil and Analog Signal Conditioning Electronics for Fluxgate Magnetometer Sensor

U. A. Sadiq[1,2,3] O. W. Oluyombo[1]
1.National Space Research & Development Agency, Abuja, Nigeria
2.Center for Satellite Technology Development, Abuja, Nigeria
3.University of Abuja, Nigeria

Abstract
The design of fluxgate magnetometers is typically a nonlinear multi-objective optimization problem. Different objectives often conflict with each other, and sometimes an optimal Fluxgate Magnetometer Sensor (FMS) performance is difficult to achieve. The sensitivity of the sensor decreases with an increase of noise level while trying to reduce the sensor dimension. Hence, there is need for a systematic optimization approach for FMS design to find its optimum performance. The combined modified multi-objective Firefly Optimization Algorithm (FOA) and systematic optimization approach is suggested to improve FMS's design in this research by simultaneously optimizing the sensitivity and noise of a FMS while the sensor core, pick-up coil, and detection circuit are minimized. The developed model allowed improved sensitivity of 86.65%, reduction of noise level by 59.97% while still keeping the sensor size small by 14.29%.
Keywords: Fluxgate magnetometer sensor, noise, sensitivity, firefly optimization algorithm.
DOI: 10.7176/ISDE/10-4-03
Publication date:May 31st 2019

1. INTRODUCTION

FMS are commonly used magnetic field sensors for measuring DC or low frequency magnetic field vectors (Lu and Huang, 2015). FMS have very high sensitivity spans a wide range from 100 pT to 100 μT (Lv and Liu, 2013), low noise, small size, small power requirements, and high temperature stability (Frydrych *et al.,* 2014). Moreover, the advancements in magnetic materials which form the heart of FMS and characterize their sensitivity, noise level, and linearity range responsible for their popularity among other competitive magnetic field sensors (Can and Topal, 2015). These make them one of the magnetic field sensors that still attract the attention of many researchers because of their wide applications (Todaro *et al.,* 2012) in space research and navigation systems (Indrasari *et al.,* 2012), particularly in Earth's magnetic field exploration surveys (Kim *et al.,* 2013; Lv and Liu, 2014).

In order to optimize the performance of magnetometers, different optimization techniques for their structures and core materials had been developed. For example, the conventional approach was based on Part-by-Part Optimization (PPO) technique, which includes designing the sensor core first, then select the dimension of pick-up coil, and finally develop a low noise detection circuit. However, PPO technique is too slow, time consuming, and expensive (Grosz and Paperno, 2012). Another optimization technique for the magnetometer parameters proposed by Chen *et al.,* (2011) and Grosz *et al.*, (2011) was based on an analytical model, which was numerically solved to obtain improved large set of parameters such as volume and weight of pick-up coil, power consumption, and the noise of the signal conditioning circuit. However, the analytical optimization technique becomes unnecessarily complex when performing large number of numerical calculations to optimize the magnetometer, hence, introducing difficulty in interpreting the results obtained (Grosz and Paperno, 2012). Recently, optimization of Fluxgate Magnetometer Sensors (FMS) had been based on Finite Element Method (FEM) by using simulation software such as ANSYS, FEMM, Flux 2D, and others. On the other hand, most of these tools could not offer the users the ability to fully express their optimization purposes by formulating the objective functions (Kim *et al.,* 2013).

Driving the excitation coil and detecting the pick-up coil signal require careful design of the excitation and detection electronics circuits (Baschirotto *et al.,* 2010; Velasco *et al.,* 2011). In most literatures, the excitation circuits for fluxgate sensors are typically based on a sinusoidal (Zorlu *et al.,* 2010), triangular (Baschirotto *et al.,* 2010) or pulsed excitation (Waheed and Rehman, 2011). The pulsed excitation is easier to generate than sinusoidal or triangular excitation (Ripka, 2001) and represents a trade-off between the sensitivity and power consumption (Cui, 2013). A pulsed excitation reduces power consumption at the expense of low sensitivity (Baschirotto *et al.,* 2010; Cui, 2013).

The block diagram of the entire fluxgate magnetometer is shown in Figure 1. To periodically saturate the ferromagnetic material, the excitation signal is fed into the excitation coil of the fluxgate sensor with a square excitation current waveform with excitation frequency *f*. The pick-up coil of the FMS detects the signal by the

rising and falling edges of core magnetizing current (see Figure 2.6(c)). The pick-up coil is fed into a pre-amp with mild tuning to the second harmonic (*2f*) of the excitation frequency because the second harmonic fluxgate magnetometers produce the highest sensitivity and the lowest noise (Lu and Huang, 2015). Therefore, it is possible to extract the information on the external magnetic field by a synchronous demodulation (Miles *et al.,* 2013). Demodulation is usually accomplished with a phase sensitive detector, typically, a CMOS analogue switch following the pre-amp (Tumanski, 2013).

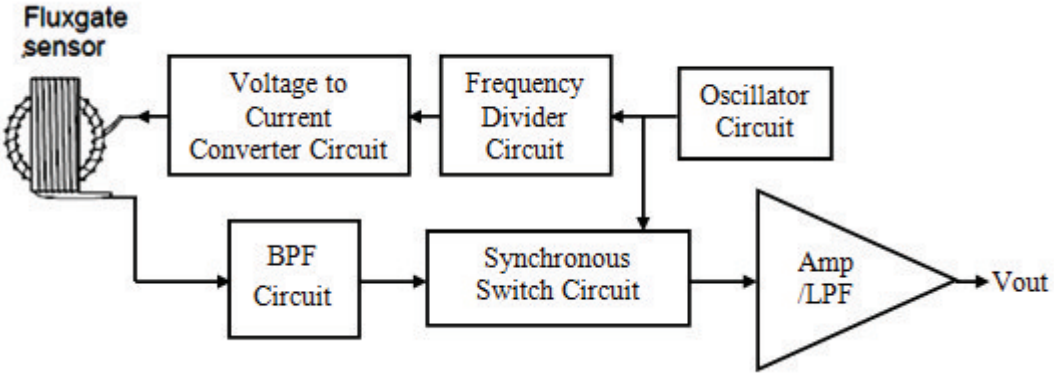

Figure 1: Typical Second Harmonic Demodulator Scheme

In this paper, the design of fluxgate magnetometers is assumed to be a nonlinear multi-objective optimization problem. Different objectives often conflict with each other, and sometimes optimal magnetometer performance is not achieved. Metaheuristic algorithms are very powerful in dealing with non-linear multi-objective optimization problem (Yang, 2013). The multi-objective Firefly Optimization Algorithm (FOA) was proposed in this research, because FOA is one of the nature-inspired metaheuristic algorithms, which is capable of handling the design problems in electromagnetics with a large number of design variables and multiple objectives under complex nonlinear constraints (Yang, 2013). For instance, sensitivity and noise of a fluxgate magnetometer can be improved while the sensor core, pick-up coil, and detection circuit are minimized. The combined multi-objective FOA and systematic optimization approach is suggested to improve FMS's design in this work by simultaneously finding the dimensions and geometry of the sensor core, pick-up coil, and detection circuit in order to reduce its noise and increase its sensitivity.

2. SYSTEM DESIGN

2.1Square Wave Current Generator

Frequency generator circuit was designed using different electronics components such as operational amplifier, transistors, hex inverters, and so on. The IC 4069 is a CMOS logic chip having six independent inverters (Fairchild, 2002). It was used for interfacing and to make simple square wave generators as shown in Figure 2.

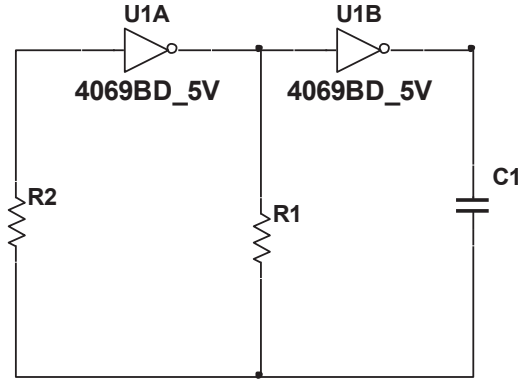

Figure 2: Schematic Diagram of a Square Wave Generator

The frequency determined by R_1 and C_1 (Fairchild, 2002) is:

$$F = \frac{1}{1.39 \times R_1 \times C_1} \quad (1)$$

Where F is the frequency in Hz, R_1 is the timing resistor in ohms and C_1 is the timing capacitor in Farad.

As shown in Figure 2, the circuit used a few components such as two resistors with R_1 used as timing resistor and a capacitor C_1 and consumes less power. The output frequency produced by the square wave oscillator depends on two components R1 and C1. Changing the values of the resistor R1 and capacitor C1 will result in change of output frequency.

2.2 Voltage to Current Converter

The frequency divider output produce analog output voltage but the current was weak and cannot be directly used to drive the magnetic core to saturation. The oscillator and the frequency divider can only produce a few tens of milli-amperes at most, while the sensor core requires many amperes. Hence, there is need for current amplification by using power transistors. Therefore, a complementary emitter-follower is commonly used for efficient bipolar current amplification. Figure 3 shows a low-noise class-AB power amplifier using NPN and PNP transistors Q1 and Q2 respectively. The two transistors Q1 and Q2 were configured as a complementary emitter-follower. Class AB amplifier is very similar to class B amplifiers, but their performance is improved by the addition of two diodes that eliminate the crossover region and allows both transistors to be turned on at the same time. The efficiency (around 50%) is not as high as class B because both transistors are turned on simultaneously, but accuracy is improved. It is the most commonly used voltage to current converter amplifier.

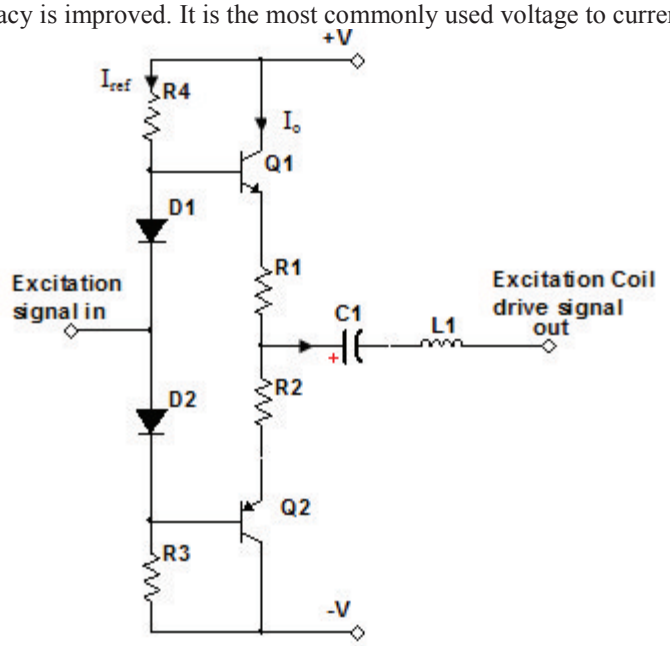

Figure 3: Schematic Diagram of a Voltage to Current Converter

As shown in Figure 3, resistor R4 and diode D1 biased the NPN transistor Q1 while D2 and R3 biased the transistor Q2. The values of the biasing resistors R3 and R4 are calculated as:

$$R_4 = \frac{V_{cc} - V_{be}}{I_{ref}} \quad (2)$$

Where R4 is a bias resistor and R3 is equal to R4. V_{cc} is the supplied voltage, V_{be} is the emitter-base voltage and I_{ref} is the transistor base bias current.

Resistors R1 and R2 are equal in values and set the operating current for the output of the transistors. The values of the emitter biasing resistors R1 and R2 are calculated as:

$$R_1 = \frac{V}{I_o} ln\left(\frac{I_{ref}}{I_o}\right) \quad (3)$$

Where R1 is an emitter bias resistor and R1 is equal to R2. V is the supplied voltage, I_o is the output current, and I_{ref} is the transistor base bias current.

The two diodes serve to bias the transistors and reduce the cross-over distortion that occurs when the input waveform crosses zero. Without the diodes, the oscillator output would have to swing 1.4V to turn one transistor on and then bring the other transistor off.

Connecting the excitation circuit to the excitation coil requires coupling capacitor that serves to isolate the AC signal from any DC bias voltages. In order for a coupling capacitor to operate effectively, it must have the right size. Capacitor C1 served to block the DC component of the current source from reaching the excitation resonant circuit. The equation to calculate the value of the coupling capacitor C_1 is:

$$C_1 = \frac{1}{3.2 f_{exc} R_{coil}} \quad (4)$$

Where C is the capacitance in Farads, and f_{exc} is the excitation signal frequency in Hertz. R_{coil} is the impedance on the load side of the capacitor which in this case is the excitation coil resistance.

As shown in Figure 3, when transistor Q1 is turned on, capacitor C3 is charged smoothly as the charging current is limited by inductor L1. The main function of the inductor L1 is to limit the current drawn from the source for the fluxgate excitation current. This was achieved by the use of a high impedance (larger than the

fluxgate sensor) inductor, which operates in the non-saturated mode over part of the excitation period. In the non-saturated state, the high impedance of the inductor limits the current flowing from the source to the excitation circuit.

2.3 Detection Electronics

The pick-up coil of the fluxgate sensor detects the signal induced by the flux collapse (saturation) and flux recovery (de-saturation) of the core magnetizing current (Evans, 2006). This small induced voltage output signal of the pick-up coil was detected and it was compensated by amplifying and filtering the signal. The second harmonic component of the induced voltage across the pick-up coil was conditioned by using the electronics circuit shown in Figure 4.

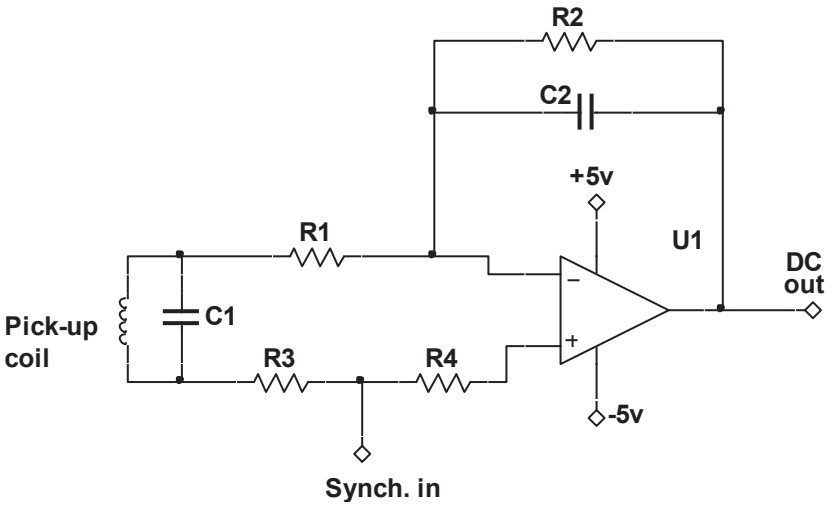

Figure 4: Schematic Diagram of Detection Electronic

The output voltage from the pick-up coil is usually small compared to the reference voltage of the Analog to Digital Converter (ADC). A low noise operational amplifier is needed to amplify the output voltage of the pick-up coil. As shown in Figure 4, at very low frequencies (within the cut-off frequency or frequency response of the amplifier), the capacitor C2 is an open circuit and the gain of the signal conditioning circuit was high, which made it acted as an amplifier. In order to evaluate the performance of FMS associated with the detection circuit, the frequency response of FMS detection amplifier was computed as (Han *et al.,* 2012; Chen *et al.,* 2015):

$$V_o = \frac{R_2}{R_1} \cdot \frac{V_{pick-up\ coil}}{1 + \left(\frac{L_w + R_2C_2}{R_1}\right) j\omega - \frac{R_2}{(R_1)} \cdot L_w C_2 \omega^2} \quad (5)$$

Where, $R_z = R_w + R_g$, R_w is the pick-up coil winding resistance, L_w is the pick-up coil inductance, C_f is the amplifier feedback capacitor, R_f is the amplifier feedback resistor.

2.4 Power Supply

To provide a stable voltage to the excitation circuit, a voltage regulator circuit was used to maintain a stable supply voltage to excitation circuit. The power supply was used to provide all the voltages necessary for driving the various components along with reference voltages. This adds up to the regulated supply voltages of +5 V, ±10 V, and ground.

3. EXPERIMENTAL SETUP

Component values were optimized to improve performance and to minimize currents in the fluxgate magnetometer. Then the circuit was tested on a breadboard and soldered on a prototyping board. After an iterative process of design optimization, the excitation frequency selected was 5 kHz square wave. The schematic diagram of the complete excitation circuit is shown in Figure 5.

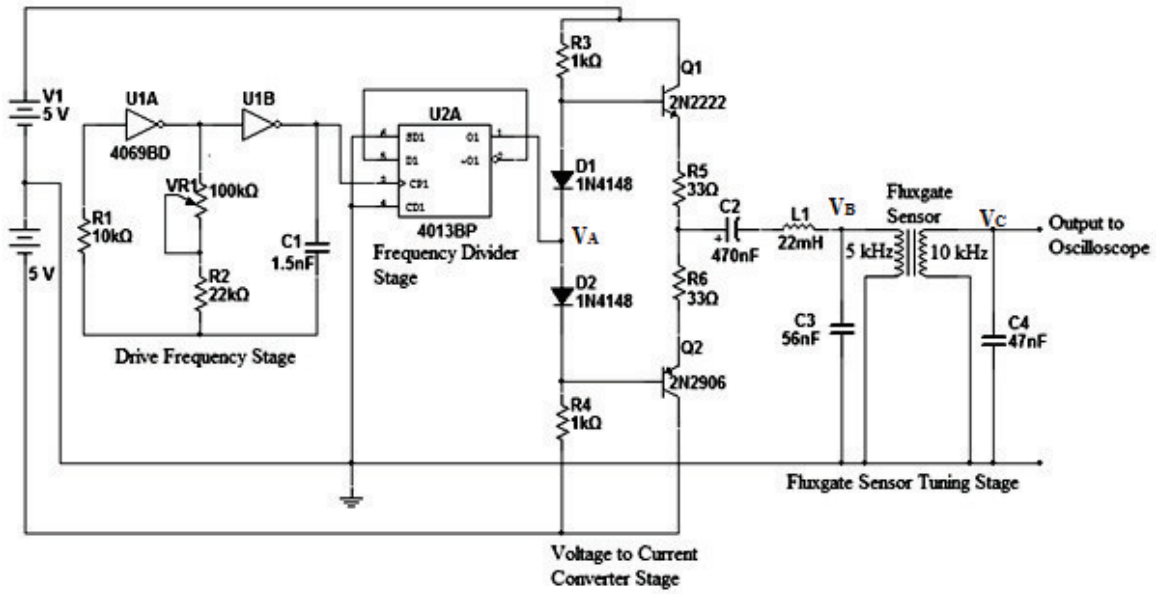

Figure 5: Driver Circuit of Developed Fluxgate Sensors

As shown in Figure 5, in order to ensure proper saturation of the ferrite magnetic core material the whole circuit was driven by a square wave oscillator at 20 kHz frequency. A duty cycle of 50% on both the 5 kHz and the 10 kHz output waveforms was ensured. A duty cycle different from 50% could compromise the demodulation of the signals produced by the sensing coils and, hence, it has to be avoided. As shown in Figure 5, by using equation (1), the oscillator block was built around resistors R1, R2 and potentiometer VR1 with capacitor C1 and Integrated Circuit (IC), hex-inverter 4069BD (U1A & U1B). The oscillator circuit was tuned to twice the excitation frequency ($2f_{exc}$) and variable between 1 kHz and 20 kHz by means of a 100 kΩ potentiometer (VR1).

The completed ring cores with excitation coils wound circumferentially were put inside a pick-up coil bobbin, which were constructed to hold the pick-up coil as shown in Figure 6. Finally, the pick-up coil with 646 turns was wound diametrically on the core with copper wire having 0.2 mm.

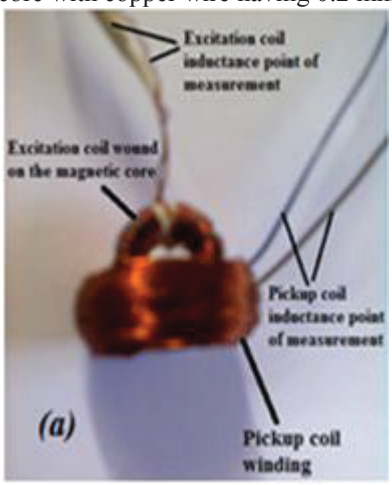

Figure 6: Prototype Sensor Coil Assembly.

As shown in Figure 6, the final dimension of the fluxgate sensor was 0.023 m × 0.02 m × 0.01 m, the dimension of the fluxgate sensor together with the printed circuit board was 0.085 m × 0.063 m × 0.01 m, while the whole system package was 0.093 m × 0.071 m × 0.022 m. The completed fluxgate sensor prototype is shown in Figure 7.

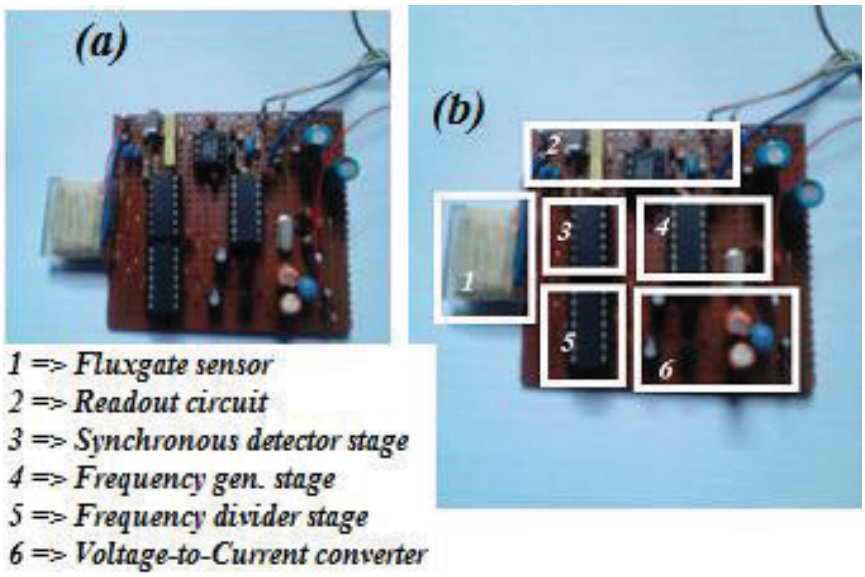

Figure 7: Complete Fluxgate Sensor System

The block diagram of the fluxgate magnetometer electronic testing board is shown in Figure 8. It consists of a 5 kHz driving oscillator, frequency divider, current booster, fluxgate sensor, synchronization circuit, and detection amplifier circuit.

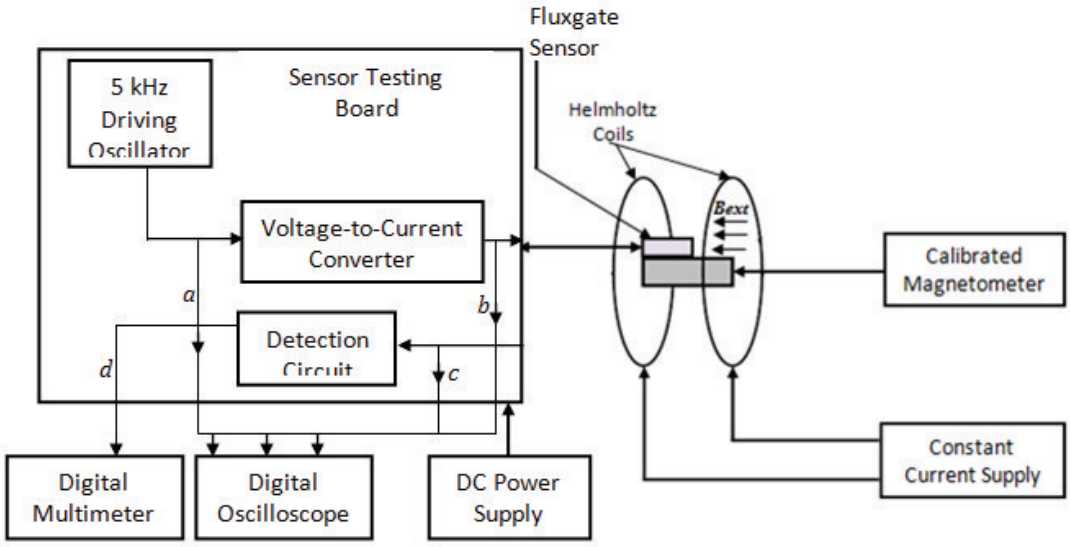

Figure 8: Block Diagram of the Experimental Setup for the Sensor Characterization.

The actual experimental setup is shown in Plate 9 with Tektronix (0-72V, 1.2A) Programmable DC Power Supply (model: PSW 4721) used to power the sensor through the testing board with the calculated excitation current of 99 mA for the sensors.

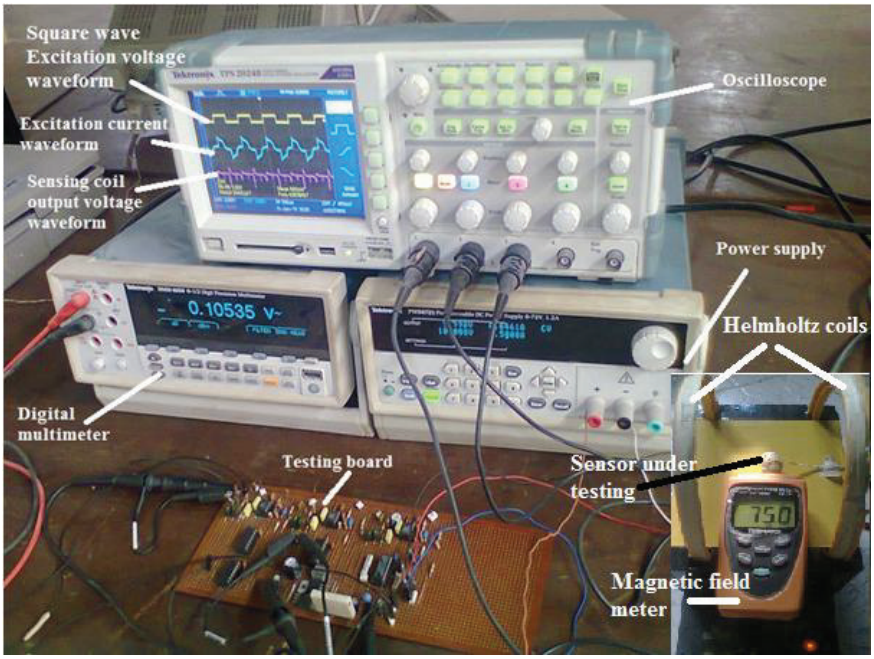

Figure 9: Actual Experimental Setup for the Characterization of the Fluxgate Sensors.

The excitation and pickup coil signal waveforms were examined by connecting the Tektronix Four Channel Digital Signal Oscilloscope (model: TPS 2024B) to the sensor excitation stage (at points a, b, and c shown in Figure 8) on the testing board. The tuned second harmonic output voltage responses of the developed FOA fluxgate sensors as a function of the applied external magnetic field were verified. As seen in Figure 9, Tektronix Digital Multimeter (2050 model) (with root mean square (rms) range selected) was connected to the pick-up coil output terminal (point 'c' shown in Figure 8) of the prototype sensors to measure the peak output voltages of the sensors corresponding to the external magnetic field supplied from the Helmholtz coil. Magnetic field strength meter (calibrated magnetometer) was used to evaluate the magnitude of the magnetic field supplied from the Helmholtz coil to the fluxgate sensors. This was done by placing the magnetic field strength meter (sensor) perpendicular to the magnetic field of the Helmholtz coil (Figure 9).

4. RESULTS

Based on the optimum values of the dimensions and geometric parameters obtained from the FOA design, FMS prototype was fabricated and studied. The sensor was made from MnZn ferrite with a thickness of 2 mm. The FOA was written in Matlab environment and the results were obtained by running the developed program on a 1.50 GHz Intel® core™ Duo CPU Windows 7 Ultimate 32-bit personal computer. The sensors were designed to withstand up to 99 mA current. Copper wire having 0.411 mm was wound as the excitation coil on each sensor with 49 turns. Parameters and the values of the FOA model are contained in Table 1.

Table 1: Optimum values of FOA Designed Sensor Parameters

Parameters	FOA Sensor	Unit
Core outside diameter	12.00	mm
Core inside diameter	8.00	mm
Core height	2.00	mm
Number of Pick-up coil turns	646	-
Pick-up Coil bobbin thickness	5.00	mm
Amplifier Feedback resistor	100.00	kΩ
Amplifier feedback capacitor	150.0	nF
Amplifier input resistor	1.80	kΩ

The measurements of the output response to field variations were made with 15 μT as the minimum magnetic field up to 75 μT maximum with step of 10 μT. The 15 μT resolution of these measurements was limited by output capability of the Helmholtz coils at the minimum driving current. It was noticed that the minimum driving current for the Helmholtz coils was 8 mA. Below this minimum driving current (8 mA), the Helmholtz coils operation became unstable resulting in the fluctuations of the output magnetic field of the calibrated magnetometer used. In addition, the 75 μT maximum magnetic fields of these measurements were limited by the induced excitation field of ±67.99 μT inside the sensor core. This was validated by the principle of fluxgate magnetometer. The smaller the sensitivity the higher the magnetic field ranges of sensor. It was noticed that the magnetic field linearity of these sensors was increasing as the core dimension was decreasing. This was

due to the increasing nature of the excitation current as the core dimension decreases which in turn increases the linearity of the sensor. Table 2 presents the tuned second harmonic output voltage obtained from the experimental measurements (Figure 9) of the pick-up coil output voltage.

Table 2: Pick-up Coil Output Voltages obtained from Measurements.

External Magnetic Field (μT)	Output Voltages (mV)
15	18.10
25	29.32
35	38.89
45	51.34
55	63.23
65	74.33
75	86.45

This data shows that the FOA simulation routine provided an accurate geometric dimension of the sensor core and the pick-up coil. During the experimental data measurements, it was observed that the sensitivity increased as the core dimension decreased up to an optimum dimension of the core at which the voltage sensitivity began to decrease.

The plot shown on Figure 10 (obtained from Table 2) shows the response of the pick-up coils of the developed sensors when tuned to second harmonic of the excitation frequency under the imposed external magnetic field from Helmholtz coils.

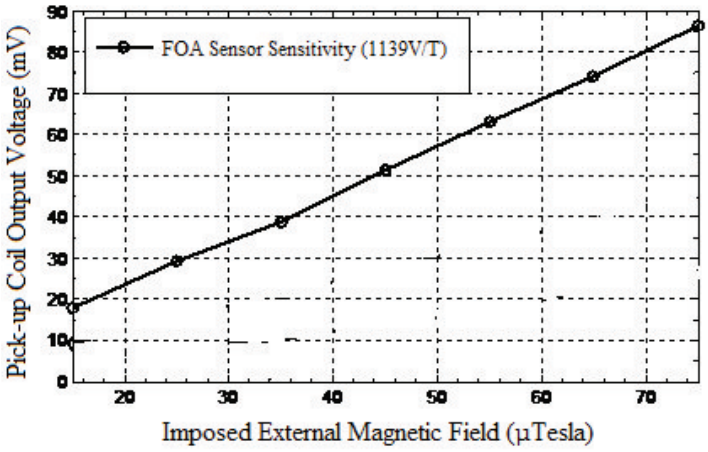

Figure 10: Fluxgate Parallel Tuned Output Plotted against External Magnetic Field.

The FMS exhibited voltage sensitivity of 1139V/T at 75μT external magnetic field range and 5 kHz excitation frequency.

Figure 11 shows the FMS responses to external magnetic field due to a bar magnet (scaled to 50μs per division on the horizontal axis and 550 mV per division on the vertical axis). These responses reflected both the influences from the applied field of a bar magnet and the remnant magnetic field. It was observed that when positive external magnetic field (North-pole of a bar magnet) was applied to the sensor, the amplitude of the pick-up coil output signal was increased and the values of magnetic field signature, S1 was higher than S2 (Figure 11).

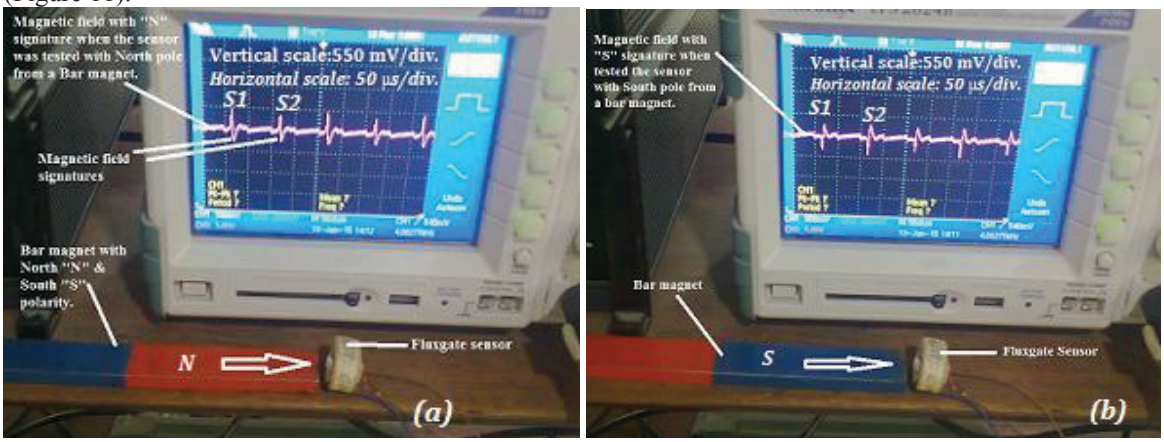

Figure 11: Magnetic Field Sensing from a Bar Magnet.

The values of the positive and negative peaks were also different. The values of the positive peaks in S1 and

S2 were 550 mV and 330 mV, respectively, while the value of the negative peaks in both S1 and S2 was 275 mV (Figure 11(a)). When negative external magnetic field (South-pole of a bar magnet) was applied to the sensor (Figure 11(b)), the amplitude of the pick-up coil output signal was also increased, but in the opposite direction and the values of magnetic field signature, S1 was smaller than S2 (Figure 11(b)). The values of the positive and negative peaks were different too. The value of the positive peaks in both S1 and S2 was 275 mV (Figure 11(a)), while the values of negative peaks in S1 and S2 were 330 mV and 550 mV, respectively. These observations could be due to the simultaneous decreased permeability of the hysteresis loop in both reverse and forward magnetization curves.

5.CONCLUSION

In this research activity, a miniature fluxgate magnetometer with magnetic ring core in a square cross section of 2 mm was realized. The sensor was wire-wound based on traditional technology process. The signal conditioning of the developed modified FOA fluxgate sensor was done by external electronics circuits. A square wave excitation current produced by a frequency oscillator circuit was fed to the excitation coil. The Helmholtz coils produced the external magnetic field to be measured. The second harmonic frequency of the induced voltage across the pick-up coil was measured with detection electronic circuit synchronized with the reference frequency from the square wave oscillator.

The introduction of the combined Firefly Optimization Algorithm (FOA) and the systematic optimization approach to FMS design problem in this research, by simultaneously finding the optimum dimensions and geometry of the sensor core, pick-up coil, and detection circuit, significantly improved the matching of the excitation and detection circuits. The developed optimized sensor for earth's magnetic field exploration showed good sensitivity of 97.09 mV/μT and linearity in the range of about ±49.44 μT. The power consumption of the sensor was 131 mW, the sensor electronics consumed 315 mW, while the whole sensor system consumed 446 mW. Hence, good sensitivity and the possibility of detecting magnetic field along two perpendicular directions make the developed FOA-based sensor suitable for portable compass application.

REFERENCES

Baschirotto, A.; Dallago, E.; Ferri, M.; Malcovati, P.; Rossini, A. and Venchi, G. (2010). A 2D micro-fluxgate earth magnetic field measurement system with fully automated acquisition setup, *Measurement*, *43*(1)/46-53.

Can, H. & Topal, U. (2015). Design of ring core fluxgate magnetometer as attitude control sensor for low and high orbit satellites. *Journal of Superconductivity and Novel Magnetism. 28*/1093-1096.

Chen, C.; Liu, F.; Lin, J. and Wang, Y. (2015). Investigation and optimization of the performance of an air-coil sensor with a differential structure suited to helicopter TEM exploration. *Sensors*, *25*/23325-23340.

Cui, Z. J. (2013). Design of a novel excitation circuit for low perming error fluxgate. *Advanced Materials Research, 748*/859-863.

Fairchild Semiconductor (2002). CD4049 Hex Inverting Buffer Manual. Fairchild Semiconductor Corporation.

Frydrych, P.; Szewczyk, R. and Salach, J. (2014). Magnetic fluxgate sensor characteristics modeling using extended preisach model. *Proceedings of the 15th Czech and Slovak Conference on Magnetism,* Kosice, Slovakia. *126*(1)/18-19.

Grosz, A. and Paperno, E. (2012). Analytical optimization of low frequency search coil magnetometers. *IEEE Sensors Journal, 12(8)*/2719-2723.

Grosz, A.; Paperno, E.; Amrusi, S. and Zadov, B. (2011). A three-axial search coil magnetometer optimized for small size, low power, and low frequencies. *IEEE Sensors Journal*, *11(4)*/1088–1094.

Han, F.; Harada, S. and Sasada, I. (2012). Fluxgate and Search Coil Hybrid: A Low-Noise Wide-Band Magnetometer. *IEEE Transactions on Magnetics*, *48(11)*/3700-3703.

Indrasari, W.; Djamal, M.; Srigutomo, W. and Ramli (2012). A magnetic distance sensor with high sensitivity based on double secondary coil of fluxgate. *IOSR Journal of Applied Physics (IOSR-JAP), 2(5)/*29-35.

Kim, Y. H.; Kim, Y.; Yang, C. S. and Shin, K. H. (2013). Optimization of operation frequency of orthogonal fluxgate sensor fabricated with Co based amorphous wire. *Journal of Magnetics, 18(2)*/159-162.

Lu, C. C. and Huang, J. (2015). A 3-Axis miniature magnetic sensor based on a planar fluxgate magnetometer with an orthogonal fluxguide. *Sensors, 15/*14727-14744.

Lv, H. and Liu, S. (2013). Research on MEMS technology of micro fluxgate sensor. *International Journal of Digital Content Technology and its Applications (JDCTA), 7(6)*/1159-1167.

Lv, H. and Liu, S. (2014). Design and fabrication of low power consumption micro fluxgate sensor. *Sensors and Transducers, 182(11)*/22-27.

Miles, D.M.; Bennest, J.R.; Mann, I.R. and Millling, D.K. (2013). A radiation hardened digital fluxgate magnetometer for space applications. *Geoscience Instrumentation Methodology Data System, 2*/213–224.

Ripka, P. (Ed), (2001). *Magnetic sensors and magnetometers*. Artech House, Boston, MA.

Tumanski, S. (2013). Modern magnetic field sensors: A Review. *Przegląd Elektrotechniczny*, *89*/1-12.

Velasco, Q. G.; Román, L. M.; Conesa, R. A. and Jeréz, F. (2011). Design of a low-consumption fluxgate transducer for high-current measurement applications. *IEEE Sensors Journal*, 11(2)/280-287.

Waheed, O.T. and Rehman, A. (2011). Design and development of a fluxgate magnetometer for small satellites in low earth orbit. *Journal of Space Technology*, 1(1)/78-82.

Yang, X.S. (2013). Multi-objectives firefly algorithm for continuous optimization. *Engineering Computation*, *29*/175–184.

Zorlu, O.; Kejik, P. and Teppan, W. (2010). A closed core micro-fluxgate sensor with cascaded planar FeNi rings. *Sensors and Actuators A, 162*/241–247.